

Article

Study on Green Controllable Preparation of Coal Gangue-Based 13-X Molecular Sieves and Its CO₂ Capture Application

Dawei Yi ¹, Huiling Du ¹, Yefei Li ^{2,*}, Yimin Gao ^{2,*}, Sifan Liu ^{1,3}, Boyang Xu ¹, Haoqi Huang ¹ and Le Kang ¹

¹ College of Materials Science and Engineering, Xi'an University of Science and Technology, Xi'an 710054, China; yidawei19820608@163.com (D.Y.); hldu@xust.edu.cn (H.D.); sifan433320@163.com (S.L.); xuboyanglwz@163.com (B.X.); g2huanghaoqi@163.com (H.H.); kangle20140805@126.com (L.K.)

² State Key Laboratory for Mechanical Behavior of Materials, College of Materials Science and Engineering, Xi'an Jiaotong University, Xi'an 710049, China

³ Shaanxi Longmen Iron and Steel Co., Ltd., Hancheng 715400, China

* Correspondence: liyefei@xjtu.edu.cn (Y.L.); ymgao@xjtu.edu.cn (Y.G.)

Abstract: Carbon dioxide emissions are the primary and most direct contributor to global warming, posing a significant hazard to both the environment and human health. In response to this challenge, there has been a growing interest in the development of effective carbon capture technologies. This study involved the synthesis of 13-X molecular sieve porous materials using solid waste coal gangue as a source of silicon and aluminum. The synthesis process involved the controlled utilization of an “alkali fusion-hydrothermal” reaction system. The resulting materials were characterized for their structure, morphology, and crystal composition using X-ray diffraction and field emission scanning electron microscopy. These 13-X molecular sieve materials were employed as adsorbents to capture carbon dioxide gas, and their adsorption performance was investigated. The findings indicated that the 13-X molecular sieve materials possess uniform pores and complete crystalline morphologies, and they exhibited an adsorption capacity of 1.82 mmol/g for carbon dioxide at 0 °C. Consequently, this study not only converted solid waste gangue into high-value products but also demonstrated effective atmospheric carbon dioxide capture, suggesting that gangue-based 13-X molecular sieves may serve as a potential candidate for carbon capture.

Keywords: coal gangue; hydrothermal synthesis; 13-X molecular sieve; CO₂ capture



Citation: Yi, D.; Du, H.; Li, Y.; Gao, Y.; Liu, S.; Xu, B.; Huang, H.; Kang, L. Study on Green Controllable Preparation of Coal Gangue-Based 13-X Molecular Sieves and Its CO₂ Capture Application. *Coatings* **2023**, *13*, 1886. <https://doi.org/10.3390/coatings13111886>

Academic Editors: Alexander S. Leshin and Vladimir Kashkarov

Received: 19 September 2023

Revised: 28 October 2023

Accepted: 29 October 2023

Published: 2 November 2023



Copyright: © 2023 by the authors. Licensee MDPI, Basel, Switzerland. This article is an open access article distributed under the terms and conditions of the Creative Commons Attribution (CC BY) license (<https://creativecommons.org/licenses/by/4.0/>).

1. Introduction

One of the primary contributors to global warming is the substantial volume of carbon dioxide emissions resulting from human activities, such as the combustion of coal and natural gas for electricity generation [1]. Over the past few centuries, atmospheric CO₂ levels have risen dramatically to 418 ppm, doubling global CO₂ emissions compared to the 1970s. This has led to the production of approximately 3.2 billion tons of CO₂ annually and a 1.5 °C increase in global average temperatures, exerting significant pressure on environmental management [2–5]. Records show that even within indoor spaces, CO₂ concentrations continue to rise, posing long-term threats to human health, travel, food, security, water resources, the rising sea level, and biodiversity [6–8]. Consequently, there is a need to control CO₂ levels and research effective methods for capturing CO₂ from the atmosphere, with adsorption technology emerging as a promising avenue due to its versatility and applicability [9,10]. Currently, available adsorbents include activated carbon [11,12], graphene [13,14], metal oxides [15], metal–organic frameworks [16,17], and zeolites [18–20], all possessing CO₂ adsorption sites within their crystal structures. In light of these pressing challenges, it is imperative to urgently address the rising atmospheric CO₂ concentrations.

Molecular sieves, also known as zeolites, are crystalline silica–aluminates composed of [SiO₄]^{4−} and [AlO₄]^{5−} tetrahedra, forming three-dimensional spatial network structures

with abundant fixed-pore size channels or cage structures [21–23]. These unique pore structures and large surface areas make them valuable in the realm of adsorbents [24–26]. As coal remains a major energy source, a substantial amount of coal gangue is produced during coal mining and washing processes. It is estimated that global coal production and consumption reached 8.1 billion tons and 15.7 billion tons, respectively, in 2019 since the 18th century [27,28]. Coal gangue (CG), a byproduct of coal mining, is associated with coal and yields 100–150 kg of gangue for every ton of coal produced [29]. In China, the cumulative accumulation of coal gangue has reached 4.5 billion tons due to years of coal mining, with an annual growth rate of 300–350 million tons [30]. This not only occupies significant land but also leads to air and water pollution, resulting in ecological degradation and health risks [31–33]. Given that coal gangue primarily contains silica and aluminum clay minerals [34,35], it is an ideal raw material for high-purity molecular sieve synthesis, addressing the challenge of coal gangue treatment and disposal.

Addressing these challenges, this study focused on the preparation of gangue-based 13-X molecular sieve porous materials using coal gangue as a source of silicon and aluminum. Optimal synthesis conditions for 13-X molecular sieves were explored, including Si/Al ratio (PCG to NaAlO₂ mass ratio), alkalinity (NaOH(aq) concentration), crystallization temperature, and hydrothermal time. The resulting molecular sieve porous materials exhibited excellent CO₂ adsorption performance, offering a sustainable solution to both coal gangue accumulation and the increase in atmospheric CO₂ concentrations, promoting circular economy and waste management objectives.

2. Experiment

2.1. Materials

In the experiment, coal gangue was used as raw material to provide silicon and aluminum sources, and it was provided by China Shaanxi Shendong Coal Mining Group of Shaanxi Province, China. Sodium hydroxide (NaOH, AR, ≥99.70%) and sodium meta-aluminate (NaAlO₂, AR, ≥99.70%) were purchased from Tianjin Damao Chemical Reagent Factory. The experimental water was homemade deionized water prepared in the laboratory. All chemical reagents were used as they were without further purification.

2.2. Methods

2.2.1. Synthesis of Gangue-Based 13-X Molecular Sieve

The crystal structure of inert amorphous quartz and kaolinite in raw coal gangue is decomposed in the strong alkali environment and participates in the chemical reaction to produce soluble aluminosilicate Na₂SiO₃ and NaAlO₂, eliminating the influence of quartz and kaolinite on the purity of the product. Through the preliminary experiment, the best ash-to-alkali ratio of pre-treated coal gangue has been explored, and the treatment methods are as follows: The raw coal gangue powder was mixed with solid NaOH particles by mass ratio of 1:0.6 in a mortar and ground thoroughly, placed in a muffle furnace, and calcined at 750 °C under air conditions for 4 h to obtain pretreatment gangue (PCG). PCG (7.0 g) and NaAlO₂ (1.17 g) were added to NaOH solution (0.3 mol·L⁻¹, 75 mL). Then, the stirred mixture was subjected to hydrothermal synthesis reaction at 80 °C for 10 h in stainless steel PTFE reactor liner; after the reactor cooled naturally, the hydrothermal products were filtered, washed, and dried to synthesize 13-X molecular sieve, and Figure 1 shows the flow chart of molecular sieve preparation.

In the context of adsorbing airborne substances, most adsorbents are in granular form, necessitating the transformation of powdered molecular sieve materials into granules [36,37]. The synthesized 13-X molecular sieve powder is initially washed to achieve a pH of approximately 7 and dried at 60 °C for 3–4 h. Subsequently, the powder is compressed into cylinders under a pressure of 20–30 MPa, and particles with diameters ranging from 1 to 3 mm are obtained through crushing and sieving. In the adsorption experiments, ultra-high purity CO₂ (U-Sung, 99.999%) is utilized, and the molecular sieve particles undergo evacuation at temperatures between 200 and 250 °C prior to measurement.

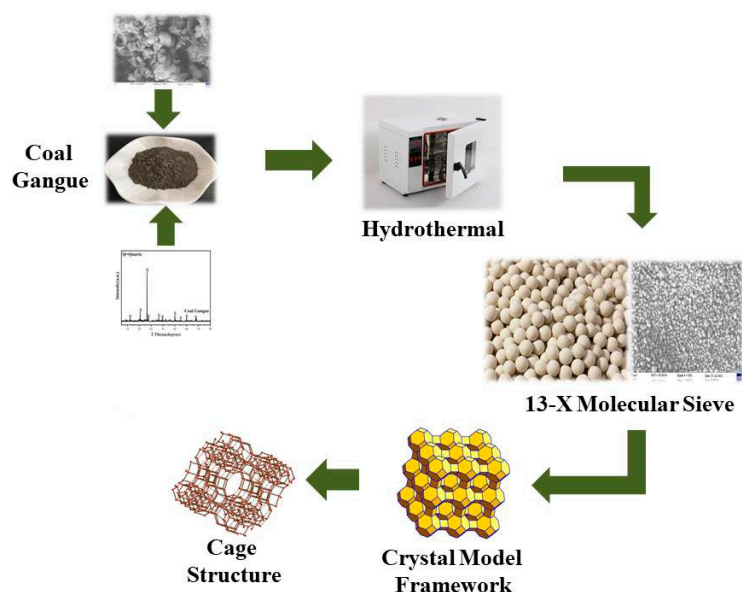


Figure 1. Flow chart of preparation of gangue-based 13-X molecular sieve.

2.2.2. Characterization

X-ray fluorescence spectrometer (XRF, Bruker S4 pioneer, Karlsruhe, Germany) was used to determine the chemical composition of the gangue for quantitative analysis. The crystallinity of the samples was evaluated by physical phase retrieval on a Bruker D8-FOCUS type X-ray diffractometer with a scanning speed of $5^\circ/\text{min}$ and a scanning angle of $5^\circ\sim 80^\circ$. Field emission scanning electron microscopy (FESEM, Gemini SEM 500, Hitachi, Japan) was used to observe the microstructure and surface morphology of the samples, and the microanalysis was determined by energy spectrum analysis (EDS). The specific surface area and pore size distribution of the samples were obtained using the N_2 adsorption–desorption isotherm at 77 K of liquid nitrogen temperature using Micromeritics ASAP 2020 analyzer (Micromeritics, Norcross, GA, USA). The CO_2 gas adsorption–desorption isotherms of 13-X molecular sieve were measured on a Quantachrome version 5.21 gas adsorption analyzer.

3. Results and Discussion

3.1. Processing and Analysis of Raw Materials

3.1.1. Treatment of Raw Material Gangue

To enhance the crystallinity of the molecular sieve, coal gangue is initially crushed using a crusher and ball mill, followed by sieving through a 200 mesh sieve to obtain gangue powder. The primary components of the gangue are silicon and aluminum compounds, with negligible quantities of other compounds. Chemical composition analysis was conducted using X-ray fluorescence spectrometry (XRF, Bruker S4 pioneer, Germany), revealing that the gangue is primarily composed of SiO_2 and Al_2O_3 , along with trace oxide impurities containing Ca, Mg, K, Fe, Na, and other elements, as well as some organic carbon (Table 1). The XRD pattern of the gangue indicates that its main mineral composition is quartz (Figure 2). Field emission scanning electron microscopy (FESEM) images demonstrate that the raw material consists of irregular lumps or agglomerates with non-uniform particle size distribution and a significant presence of non-crystalline particulate matter on its surface.

Table 1. Chemical composition of coal gangue.

Oxide	CaO	MgO	SiO_2	Al_2O_3	Fe_2O_3	TiO_2	K_2O	Na_2O	Loss
wt%	0.82	1.57	61.39	23.76	4.14	0.79	2.82	1.62	2.11

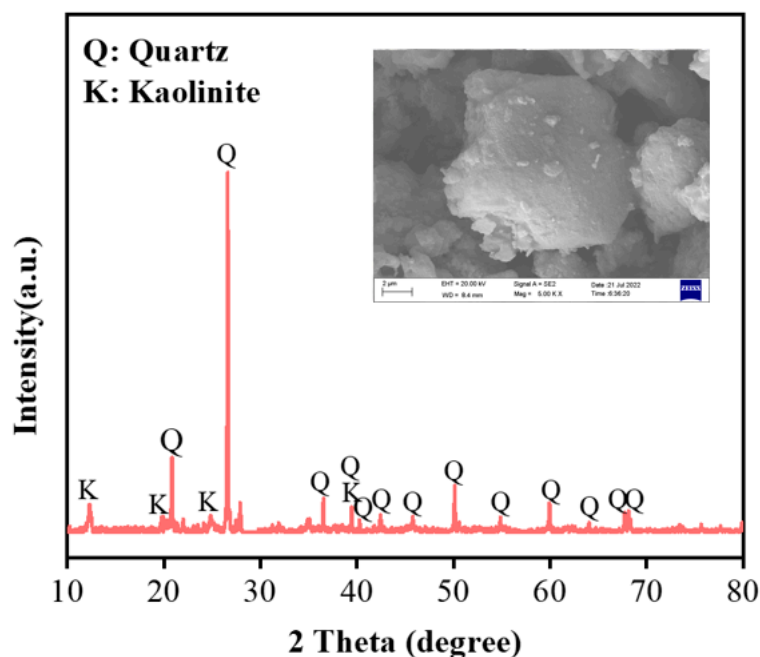


Figure 2. XRD pattern and FESEM pattern of coal gangue.

3.1.2. Orthogonal Experimental Design for the Synthesis of 13-X Molecular Sieve

In this study, there are many factors affecting the preparation of a 13-X molecular sieve, and an orthogonal test can conduct a comprehensive experiment on the collocation between various levels of each factor, so an orthogonal test is chosen as the research method. After the preliminary exploration experiment, the influence factors and levels of the experiment were controlled at four factors and three levels, and the orthogonal table $L_9(3^4)$ was selected, as shown in Table 2 below.

Table 2. Orthogonal experimental scheme.

Serial Number	Influence Factor			
	Si/Al (PCG/NaAlO ₂ Mass Ratio)	Alkalinity (C _{NaOH(aq)})/mol·L ⁻¹	Crystallization Temperature/°C	Hydrothermal Time/h
Y1	4	0.3	100	8
Y2	4	0.4	120	10
Y3	4	0.5	80	12
Y4	5	0.5	100	10
Y5	5	0.3	120	12
Y6	5	0.4	80	8
Y7	6	0.4	100	12
Y8	6	0.5	120	8
Y9	6	0.3	80	10

This study explored the impact of four key factors, Si/Al ratio (PCG to NaAlO₂ mass ratio), alkalinity (NaOH(aq) concentration), crystallization temperature, and hydrothermal time, on the crystallinity of gangue-based 13-X molecular sieve products. The synthesized samples were denoted as Y1, Y2–Y9, etc.

3.2. Evaluation of the Synthesized 13-X Zeolite

3.2.1. X-ray Diffraction Analysis

The influence of the Si/Al molar ratio on the crystallization type of molecular sieve was examined. The coal gangue exhibits a high content of SiO₂ and Al₂O₃, with an n(Si)/n(Al) ratio of 2.20. Given that the X-type molecular sieve is considered a low-silica molecular sieve, the raw coal gangue is well-suited for the synthesis of low-silica molecular sieve

porous materials with high crystallinity. The XRD spectra of synthetic samples Y1–Y9 were compared with standard 13-X molecular sieve values (PDF#12–0246) (Figure 3). Samples Y7 and Y9 exhibited distinct peaks at 2θ of 6.090° , 9.998° , 11.696° , 15.424° , 20.073° , 23.310° , and 31.015° , indicating the presence of 13-X molecular sieve diffraction peaks. Other synthetic samples did not exhibit a 13-X molecular sieve, but the amorphous silicate content within the raw material system increased, and the quartz phase diminished as the reaction progressed. This transformation was due to the interaction of alkaline substances with the quartz crystalline phase on the gangue's surface, leading to structural alterations. These findings underscore the significance of the SiO_2 and Al_2O_3 ratio in the parent composition in determining the molecular sieve structure type.

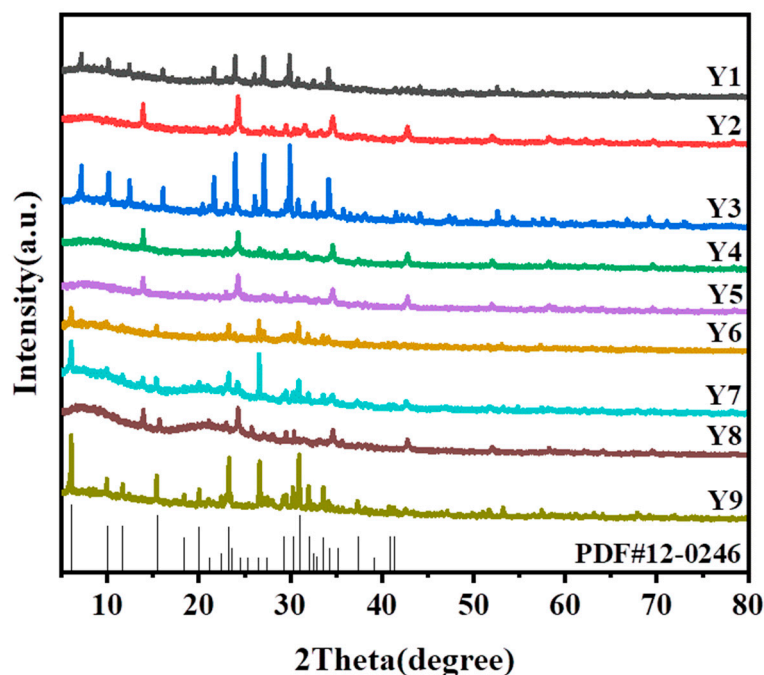


Figure 3. XRD patterns of the synthesized samples Y1–Y9 and 13-X standard card (bottom of the image).

The impact of alkali addition on the synthesized products was also analyzed, showing that the addition of an alkali source effectively disrupted the inert crystal structure of quartz in the gangue, enabling the dissolution of active silicoaluminate components. Alkalinity, determined by different alkali concentrations, significantly influenced the crystallinity of molecular sieves. In samples with a Si/Al molar ratio (PCG to NaAlO_2 mass ratio = 6), varying NaOH solution concentrations (0.4 , 0.5 , and $0.3 \text{ mol}\cdot\text{L}^{-1}$) were tested. Samples Y7 and Y9, which exhibited the diffraction peaks of a standard 13-X molecular sieve, indicated that higher NaOH addition was not conducive to 13-X molecular sieve nucleation. An increase in alkalinity led to a gradual reduction in the diffraction intensity of the 13-X molecular sieve. Sample Y8 had excessively high alkalinity, resulting in a highly basic crystallization reaction process. Consequently, it hindered silicate ion polymerization and produced different structures. The synthesis of molecular sieves through alkali fusion and appropriate alkalinity adjustment treatments promoted the depolymerization of Si–Al radical ions and facilitated zeolite grain formation and crystal growth. Different NaOH ratios yielded distinct crystal structures, with a material concentration of $0.3 \text{ mol}\cdot\text{L}^{-1}$ providing well-developed 13-X molecular sieves. This sufficient alkalinity promoted the uniform nucleation of pure 13-X zeolites and supplemented the sodium content in the molecular sieves.

The synthesis of molecular sieves involves a process of silica–aluminate precipitation in an alkali solution, and changes in crystallization temperature affect the interaction between silica–aluminate and $[\text{SiO}_2(\text{OH})_2]^{2-}$ and $[\text{Al}(\text{OH})_4]^-$. To investigate the impact

of different crystallization temperatures on the synthesis of 13-X molecular sieves, three series of syntheses were conducted at 80 °C, 100 °C, and 120 °C. As shown in Figure 3, when the crystallization temperature was set at 120 °C, the formation of crystals of other structures or impurities occurred, as evidenced by the absence of standard 13-X zeolite diffraction peaks and the appearance of different crystal structures. Consequently, 13-X zeolites could not be synthesized at this temperature. When the crystallization temperature was reduced to 80 °C and 100 °C, high-purity x-type zeolites were formed. Notably, 13-X zeolites synthesized at 80 °C exhibited higher efficiency, with sample Y9 approaching the relative crystallinity of standard 13-X. Therefore, considering energy conservation and maintaining the integrity of the 13-X molecular sieve's crystal structure, 80 °C is more suitable for producing high-purity 13-X zeolites.

Hydrothermal time plays a role in the growth and formation of molecular sieve crystals, and different hydrothermal crystallization times can yield various crystal structures. The effect of hydrothermal time was studied in three series, 8 h, 10 h, and 12 h, to regulate the growth and formation of synthetic 13-X molecular sieves.

The XRD spectrum in Figure 3 reveals that at a crystallization time of 10 h, sample Y9 displayed the highest crystallinity of 13-X zeolite. Subsequently, the diffraction intensity of 13-X zeolite decreased beyond 10 h, suggesting the conversion of some X zeolites into more stable zeolites as a result of increased silicon dissolution during longer hydrothermal synthesis. Therefore, precise control of hydrothermal time is crucial in the synthesis of 13-X molecular sieves, with 10 h being considered the optimal duration for the formation of crystalline 13-X zeolites.

Taking into account the Si/Al molar ratio (PCG to NaAlO₂ mass ratio = 6), a NaOH solution concentration of 0.3 mol·L⁻¹, a crystallization temperature of 80 °C, and a hydrothermal time of 10 h, the best conditions for synthesized 13-X molecular sieves were achieved. The resulting product, Y9, exhibited sharp and complete characteristic peaks, minimal amorphous peaks, and a high degree of purity in its crystalline phase.

3.2.2. SEM-EDS Analysis

The electron microscope allows observation of the surface morphology and crystal size of molecular sieves, offering insights into crystal uniformity, the presence of heterocrystals, and the overall image quality. To study the crystal pattern variations, the synthesized product is initially gently ground, pretreated, gold-sprayed, and subjected to vacuum treatment. It can be seen from Figure 3 that the XRD spectrum of the synthesized sample Y1-Y9 is compared with the standard 13-X molecular sieve value (PDF#12-0246), as shown in Figure 3. The peaks of Y7 and Y9 at the 2° curves of 6.090°, 9.998°, 11.696°, 15.424°, 20.073°, 23.310°, and 31.015° indicate that the synthesis products have 13-X molecular sieve diffraction peaks at this point. Secondly, the surface morphology and crystal size of the synthesized molecular sieve samples were observed by electron microscopy. The regular octahedral structure of the 13-X molecular sieve appeared in both the Y7 and Y9 samples, but due to the difference in the level of synthetic factors in the Y7 samples, other types of molecular sieve structures were generated. Therefore, Y7 was selected for comparison and discussion with the optimal group Y9. SEM and EDS patterns of the raw material gangue, synthesized sample Y7, and the best sample Y9 are presented in Figure 4. Figure 4a,b illustrate the microscopic morphology of raw coal gangue, displaying dark gray powder after calcination. The material exhibits various shapes and sizes of lamellar structures, with lamellae stacked together in a cascade arrangement, indicating inadequate crystallization. Figure 4c presents the EDS energy spectrum analysis of raw coal gangue, revealing the main characteristic peaks corresponding to elements that constitute the octahedral crystals of the 13-X molecular sieve. Figure 4d,e show the microscopic morphology of synthesized sample Y7, characterized by an absence of octahedral structure and irregular spherical crystal morphology with uniform particle size. This indicates that the synergistic effect of high alkalinity, a long hydrothermal time, and a high temperature is not conducive to the nucleation and crystal growth of the 13-X zeolite molecular sieve. Figure 4f displays the

EDS spectrum analysis of the Y7 sample molecular sieve. In Figure 4g,h, the microscopic morphology of the best sample, Y9, reveals ortho-octahedral molecular sieve crystals with clear angles, uniform particle size and a regular overall shape [38]. The particle size is approximately 2 μm , and there is no fuzzy colloid in the electron microscope image. Figure 4i provides the EDS energy spectrum analysis of the Y9 sample, indicating that the synthesized product Y9 molecular sieve contains elements O, Na, Al, and Si with weight percentages of 35.60, 8.24, 12.05, and 17.38, respectively. The molar ratio of Si-Al is approximately 1.4, which is close to the theoretical formula of $\text{Na}_2\text{O}\cdot\text{Al}_2\text{O}_3\cdot 2.5\text{SiO}_2\cdot 6\text{H}_2\text{O}$. These findings affirm the high quality and crystalline purity of the synthesized products.

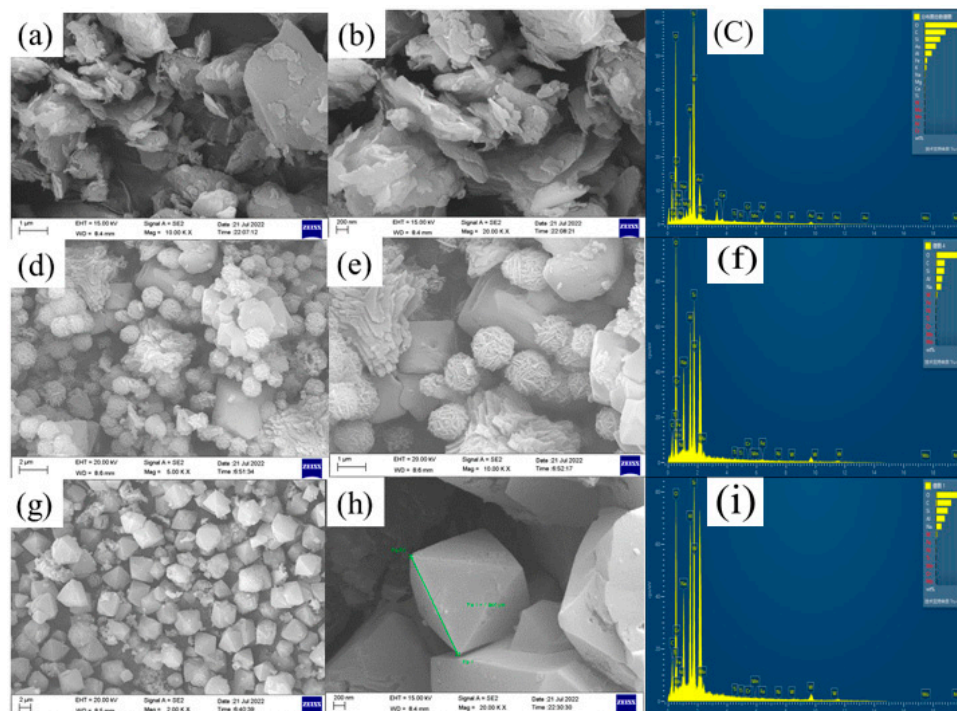


Figure 4. SEM patterns of raw coal gangue, (a,b); Y7 sample, (d,e); Y9 sample, (g,h). EDS patterns of raw coal gangue, (c); Y7 sample, (f); and Y9 sample, (i).

3.2.3. Specific Surface Area Analysis

The specific surface area is a crucial parameter for evaluating the adsorption capacity of molecular sieve porous materials. In general, a larger specific surface area indicates a stronger adsorption capacity. Table 3 presents the surface structure parameters of the coal gangue Y9 molecular sieve, with the BET method used to measure the surface area. The data in the table show that the BET-specific surface area of coal gangue is 2.04 m^2/g , with almost no adsorption capacity. After the synthesis in the alkali fusion–hydrothermal system, sample Y9's BET-specific surface area significantly increased to 377.02 m^2/g , accompanied by a qualitative improvement. The average pore size reached 2.09 nm, approximately 185 times that of the original gangue. These results demonstrate that the experimentally synthesized 13-X molecular sieve exhibits a high BET-specific surface area. Figure 5 presents the N_2 adsorption–desorption curve and pore size distribution of sample Y9, revealing increased adsorption with rising pressure. The adsorption–desorption isotherm curve resembles a typical Langmuir IV curve, indicating the presence of slit mesopores and a typical physical adsorption process. The pore size distribution of sample Y9 primarily centers on 38.8 nm mesopores, signifying a favorable pore structure. These findings confirm that the experimentally synthesized sample Y9 offers a high specific surface area and predominantly features physisorption, which is easily regenerated and recyclable, enhancing its ability to interact with adsorbents.

Table 3. Surface structural parameters of gangue, Y9 molecular sieves, and commercial 13-X molecular sieves.

Sample	BET-Specific Surface Area (m ² /g)	Average Pore Size (Å)	Pore Volume (m ³ /g)
Coal Gangue	2.04	—	—
Y9	377.02	20.87	0.20
Commercial 13-X molecular sieve	523.88	18.62	—

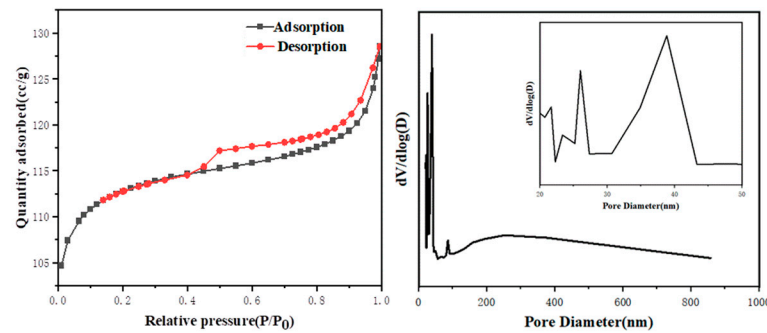


Figure 5. N₂ adsorption–desorption isotherm curve and pore size distribution of Y9 molecular sieve.

3.3. Measured Characteristics of CO₂ Adsorption by Gangue-Based 13-X Molecular Sieve

Figure 6 displays a bar graph representing the adsorption capacity of the synthesized molecular sieve for CO₂ at different temperatures. The gas adsorption process generally releases heat, making temperature a critical factor affecting molecular sieve gas adsorption. As depicted in Figure 6, the CO₂ adsorption capacity of all the synthesized molecular sieve samples, particularly Y9, diminishes as the temperature rises. The maximum CO₂ adsorption capacity of the 13-X molecular sieve is observed at 0 °C (273 K), reaching 1.82 mmol/g.

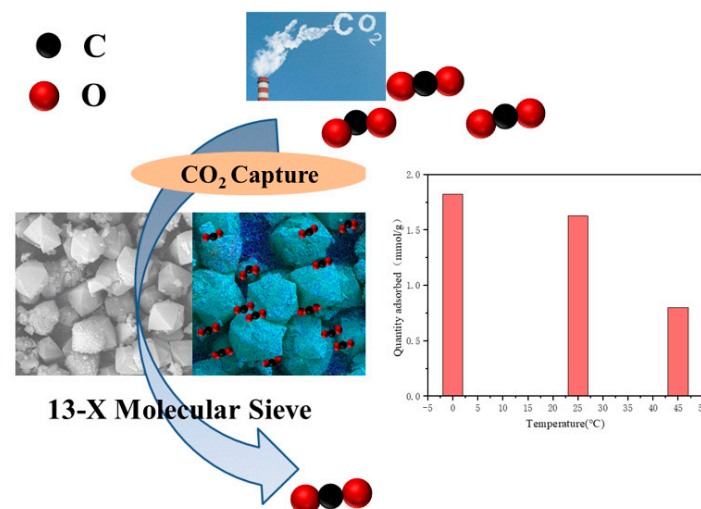


Figure 6. Column chart of CO₂ adsorption capacity of synthesized molecular sieve at different temperatures.

A number of adsorption models are commonly used to predict the adsorption of adsorbents at different pressures as a reference for further studies of the adsorption mechanism. In this study, the Langmuir Model and Dual-site Langmuir Model were used to fit the CO₂ adsorption isotherm.

Langmuir Model:

$$q = q_A \frac{b_A p}{1 + b_A p} \tag{1}$$

Dual-site Langmuir Model:

$$q = q_A \frac{b_A p}{1 + b_A p} + q_B \frac{b_B p}{1 + b_B p} \quad (2)$$

In Equations (1) and (2), q is the adsorption amount, mmol/g; p is the absolute pressure, kPa; q_A and q_B are the saturation adsorption amounts, mmol/g; b_A and b_B are the affinity constants, kPa.

Figure 7 illustrates the isothermal fitting curves for CO₂ adsorption at various temperatures for the synthesized 13-X molecular sieve Y9, employing the Dual-site Langmuir Model for fitting. Table 4 presents the correlation coefficient values of both the Langmuir Model and the Dual-site Langmuir Model. It is evident that the Dual-site Langmuir Model offers a more accurate description of the variable pressure adsorption process for CO₂ gas within the synthesized 13-X molecular sieve. As the pressure gradually increases, the two adsorption sites work synergistically, causing changes in their affinity effects. Additionally, due to the mesoporous structure of the synthesized 13-X molecular sieve, adsorption predominantly takes place within the mesopores at higher relative pressures. Inside the molecular sieve skeleton, cavities contain charge-compensating cations, resulting in the emergence of acidic sites. The negatively charged skeletal oxygen near these cations acts as a basic site, interacting with the permanent quadrupole moment in CO₂ [35], leading to higher CO₂ adsorption rates. Consequently, in conjunction with the sorption data, it was determined that continuous sorption testing at 0 °C was most suitable for various temperature conditions. In prior studies, gangue has been employed as a raw material for CO₂ adsorbent synthesis, offering cost reductions and substantial environmental benefits. This suggests the potential utility of gangue-based 13-X molecular sieves for CO₂ capture.

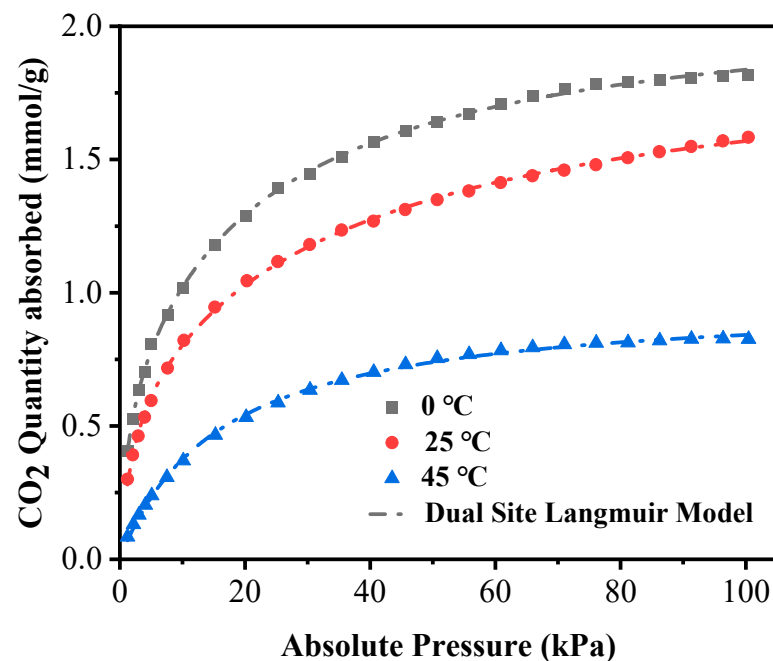


Figure 7. CO₂ adsorption isothermal fitting curves of synthesized 13-X molecular sieve Y9 at different temperatures and Dual-site Langmuir Model fitting.

The effect of synthesized 13-X molecular sieves on CO₂ adsorption performance at 25 °C was investigated at different adsorption pressures of 20 kPa, 40 kPa, 60 kPa, 80 kPa, and 100 kPa, respectively, as shown in Figure 8, which is the histogram of CO₂ adsorption capacity at different adsorption pressures. It can be observed from the figure that the adsorption capacity of 13-X molecular sieves for CO₂ showed an increasing trend with the increase of pressure. The adsorption capacity of the 13-X molecular sieve for CO₂ increased from 1.04 mmol/g to 1.27 mmol/g for pressure from 20 kPa to 40 kPa and

increased continuously with the pressure, and reached 1.58 mmol/g for the adsorption capacity at 100 kPa. The CO₂ adsorption capacity of the 13-X zeolite showed a tendency to increase and then decrease with the increase of the pressure. This indicates that the larger the adsorption pressure, the greater the influence the 13-X molecular sieve has on the adsorption capacity, and this also shows a positive correlation trend. Secondly, when the pressure increases, the asymmetric vibration of Si-O and Al-O tetrahedra in the molecular sieve will be strengthened, which makes the asymmetric vibration of Si-O and Al-O tetrahedra in the molecular sieve more obvious. The gas and water will be discharged from the pores, thus enlarging the diameter of the pores and improving the adsorption capacity of the 13-X molecular sieve for CO₂ gas.

Table 4. Isothermal model coefficients of CO₂ adsorption at different temperatures.

Temperature (°C)	Langmuir Model			Dual-Site Langmuir Model				
	q _A (mmol/g)	b _A (kPa ⁻¹)	R ²	q _A (mmol/g)	b _A (kPa ⁻¹)	q _B (mmol/g)	b _B (kPa ⁻¹)	R ²
0	1.91	0.13	0.9799	1.48	0.04	0.64	0.84	0.9995
25	1.65	0.10	0.9796	1.29	0.03	0.65	0.48	0.9994
45	0.98	0.06	0.9988	0.49	0.06	0.49	0.06	0.9988

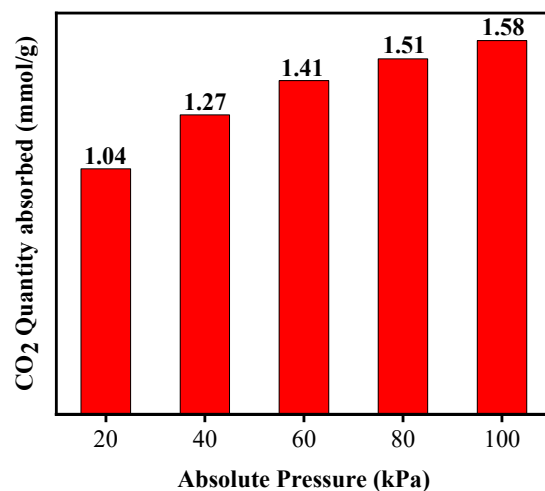


Figure 8. Column chart of CO₂ adsorption capacity under different adsorption pressures.

In order to examine the CO₂ adsorption capacity of competing adsorbents, the CO₂ capture capacity of the synthesized 13-X molecular sieve was compared with other CO₂ adsorbents reported in the literature in this study, and the results of the comparison are shown in Table 5. As can be seen from the data in Table 5, the CO₂ capture capacity of the 13-X molecular sieve synthesized in this work is close to that of adsorbents reported in the literature [39] and exceeds that of many reported CO₂ adsorbents, such as Hierarchical melamine resin sponges [40] and Amine-impregnated Silica foam [41].

Table 5. Comparison of CO₂ trapping capacity of different adsorbents.

Sample	Adsorption Temperature (°C)	Adsorption Capacity (mmol/g)	References
zeolite 13-X	0	1.8	Present work
Hierarchical melamine resin sponges	0	1.7	[40]
β-zeolite	30	1.8	[39]
Monolithic Ni/ZSM-5	35	2.4	[42]
Amine-impregnated Silica foam	25	1.48	[41]
ZSM-5	0	2.37	[43]

4. Conclusions

The 13-X molecular sieve porous materials were synthesized by alkali melting and hydrothermal treatment using cheap and readily available solid waste-based coal gangue as a raw material, without adding any silicon or alumina sources. The effects of Si/Al, alkalinity, crystallization temperature, and hydrothermal time on the synthesis of the 13-X molecular sieve were investigated using the orthogonal experimental design. The prepared 13-X molecular sieve exhibited a highly crystalline pore structure with a BET-specific surface area of 377.02 m²/g, and it showed excellent CO₂ capture capacity (CO₂ adsorption capacity of 1.82 mmol/g) at 0 °C and 1 bar. The low cost and high value-added availability of coal gangue and the high CO₂ capture performance of coal gangue-based 13-X molecular sieves indicated that the synthesis of 13-X zeolite for CO₂ capture from gangue is an ideal resource utilization method for coal gangue that can be used in the future.

Author Contributions: Investigation, Y.L.; Resources, Y.G.; Data curation, S.L., B.X., H.H. and L.K.; Writing—original draft, D.Y.; Writing—review & editing, H.D. All authors have read and agreed to the published version of the manuscript.

Funding: This research was supported funded by the State Key Laboratory for Mechanical Behavior of Materials (Grant No. 20232508). the Excellent Youth Science and Technology Fund Project of Xi'an University of Science and Technology (Grant No. 6310221009), the National Natural Science Foundation of China (No. 52172099), the Basic Research Plan of Natural Science of Shaanxi Province (No. 2020JQ-754).

Institutional Review Board Statement: Not applicable.

Informed Consent Statement: Not applicable.

Data Availability Statement: Data will be made available on request.

Conflicts of Interest: The authors declare no conflict of interest.

References

1. Siegelman, R.L.; Kim, E.J.; Long, J.R. Porous materials for carbon dioxide separations. *Nat. Mater.* **2021**, *20*, 1060–1072. [[CrossRef](#)] [[PubMed](#)]
2. Gayathri, R.; Mahboob, S.; Govindarajan, M.; Al-Ghanim, K.A.; Ahmed, Z.; Al-Mulhm, N.; Vodovnik, M.; Vijayalakshmi, S. A review on biological carbon sequestration: A sustainable solution for a cleaner air environment, less pollution and lower health risks. *J. King Saud Univ. Sci.* **2021**, *33*, 101282. [[CrossRef](#)]
3. Qadir, S.; Su, H.; Li, D.; Gu, Y.; Zhao, S.; Wang, S.; Wang, S. Low-cost preferential different amine grafted silica spheres adsorbents for DAC CO₂ removal. *J. Energy Chem.* **2022**, *75*, 494–503. [[CrossRef](#)]
4. Greer, K.; Zeller, D.; Woroniak, J.; Coulter, A.; Winchester, M.; Palomares, M.D.; Pauly, D. Global trends in carbon dioxide (CO₂) emissions from fuel combustion in marine fisheries from 1950 to 2016. *Mar. Policy* **2019**, *107*, 103382. [[CrossRef](#)]
5. Jacobson, T.A.; Kler, J.S.; Hernke, M.T.; Braun, R.K.; Meyer, K.C.; Funk, W.E. Direct human health risks of increased atmospheric carbon dioxide. *Nat. Sustain.* **2019**, *2*, 691–701. [[CrossRef](#)]
6. Hanna, R.; Abdulla, A.; Xu, Y.; Victor, D.G. Emergency deployment of direct air capture as a response to the climate crisis. *Nat. Commun.* **2021**, *12*, 1–13. [[CrossRef](#)]
7. Djalante, R. Key assessments from the IPCC special report on global warming of 1.5 C and the implications for the Sendai framework for disaster risk reduction. *Prog. Disaster Sci.* **2019**, *1*, 100001. [[CrossRef](#)]
8. Wadi, B.; Golmakani, A.; Manovic, V.; Nabavi, S.A. Effect of combined primary and secondary amine loadings on the adsorption mechanism of CO₂ and CH₄ in biogas. *Chem. Eng. J.* **2021**, *420*, 130294. [[CrossRef](#)]
9. Aaron, D.; Tsouris, C. Separation of CO₂ from flue gas: A review. *Sep. Sci. Technol.* **2005**, *40*, 321–348. [[CrossRef](#)]
10. Luzzi, E.; Aprea, P.; de Luna, M.S.; Caputo, D.; Filippone, G. Mechanically coherent zeolite 13X/Chitosan aerogel beads for effective CO₂ capture. *ACS Appl. Mater. Interfaces* **2021**, *13*, 20728–20734. [[CrossRef](#)]
11. Drage, T.; Arenillas, A.; Smith, K.; Pevida, C.; Piippo, S.; Snape, C. Preparation of carbon dioxide adsorbents from the chemical activation of urea–formaldehyde and melamine–formaldehyde resins. *Fuel* **2007**, *86*, 22–31. [[CrossRef](#)]
12. Lu, C.; Bai, H.; Wu, B.; Su, F.; Hwang, J.F. Comparative study of CO₂ capture by carbon nanotubes, activated carbons, and zeolites. *Energy Fuels* **2008**, *22*, 3050–3056. [[CrossRef](#)]
13. Shang, S.; Tao, Z.; Yang, C.; Hanif, A.; Li, L.; Tsang, D.C.; Gu, Q.; Shang, J. Facile synthesis of CuBTC and its graphene oxide composites as efficient adsorbents for CO₂ capture. *Chem. Eng. J.* **2020**, *393*, 124666. [[CrossRef](#)]

14. Sun, H.; La, P.; Yang, R.; Zhu, Z.; Liang, W.; Yang, B.; Li, A.; Deng, W. Innovative nanoporous carbons with ultrahigh uptakes for capture and reversible storage of CO₂ and volatile iodine. *J. Hazard. Mater.* **2017**, *321*, 210–217. [[CrossRef](#)]
15. Przepiórski, J.; Czyżewski, A.; Pietrzak, R.; Toyoda, M.; Morawski, A.W. Porous carbon material containing CaO for acidic gas capture: Preparation and properties. *J. Hazard. Mater.* **2013**, *263*, 353–360. [[CrossRef](#)]
16. Zhao, Y.; Ding, H.; Zhong, Q. Synthesis and characterization of MOF-aminated graphite oxide composites for CO₂ capture. *Appl. Surf. Sci.* **2013**, *284*, 138–144. [[CrossRef](#)]
17. Jiang, M.; Li, H.; Zhou, L.; Xing, R.; Zhang, J. Hierarchically porous graphene/ZIF-8 hybrid aerogel: Preparation, CO₂ uptake capacity, and mechanical property. *ACS Appl. Mater. Interfaces* **2018**, *10*, 827–834. [[CrossRef](#)]
18. Choi, S.; Drese, J.H.; Jones, C.W. Adsorbent materials for carbon dioxide capture from large anthropogenic point sources. *ChemSusChem Chem. Sustain. Energy Mater.* **2009**, *2*, 796–854. [[CrossRef](#)]
19. Silva, J.A.; Schumann, K.; Rodrigues, A.E. Sorption and kinetics of CO₂ and CH₄ in binderless beads of 13X zeolite. *Microporous Mesoporous Mater.* **2012**, *158*, 219–228. [[CrossRef](#)]
20. Dabbawala, A.A.; Ismail, I.; Vaithilingam, B.V.; Polychronopoulou, K.; Singaravel, G.; Morin, S.; Berthod, M.; Al Wahedi, Y. Synthesis of hierarchical porous Zeolite-Y for enhanced CO₂ capture. *Microporous Mesoporous Mater.* **2020**, *303*, 110261. [[CrossRef](#)]
21. Ma, C.; Du, H.; Liu, J.; Kang, L.; Du, X.; Xi, X.; Ran, H. High-temperature stability of dielectric and energy-storage properties of weakly-coupled relaxor (1-x) BaTiO₃-xBi (Y1/3Ti1/2)O₃ ceramics. *Ceram. Int.* **2021**, *47*, 25029–25036. [[CrossRef](#)]
22. Xu, R.R.; Pang, W.; Yu, J.H.; Huo, Q.S.; Chen, J.S. Chemistry-zeolites and porous materials. In *Structural Analysis and Properties of Porous Materials Characterization*; Science Press: Beijing, China, 2004; pp. 145–149.
23. Ran, H.; Du, H.; Ma, C.; Zhao, Y.; Feng, D.; Xu, H. Effects of A/B-site Co-doping on microstructure and dielectric thermal stability of AgNbO₃ ceramics. *Sci. Adv. Mater.* **2021**, *13*, 741–747. [[CrossRef](#)]
24. Feng, D.; Du, H.; Ran, H.; Lu, T.; Xia, S.; Xu, L.; Wang, Z.; Ma, C. Antiferroelectric stability and energy storage properties of Co-doped AgNbO₃ ceramics. *J. Solid State Chem.* **2022**, *310*, 123081. [[CrossRef](#)]
25. Serrano, D.P.; Escola, J.M.; Pizarro, P. Synthesis strategies in the search for hierarchical zeolites. *Chem. Soc. Rev.* **2013**, *42*, 4004–4035. [[CrossRef](#)] [[PubMed](#)]
26. Deng, J.; Li, B.; Xiao, Y.; Ma, L.; Wang, C.P.; Lai-Wang, B.; Shu, C.M. Combustion properties of coal gangue using thermogravimetry–Fourier transform infrared spectroscopy. *Appl. Therm. Eng.* **2017**, *116*, 244–252. [[CrossRef](#)]
27. Li, H.; Li, M.; Zheng, F.; Wang, J.; Chen, L.; Hu, P.; Zhen, Q.; Bashir, S.; Liu, J.L. Efficient removal of water pollutants by hierarchical porous zeolite-activated carbon prepared from coal gangue and bamboo. *J. Clean. Prod.* **2021**, *325*, 129322. [[CrossRef](#)]
28. Guo, Y.; Yan, K.; Cui, L.; Cheng, F. Improved extraction of alumina from coal gangue by surface mechanically grinding modification. *Powder Technol.* **2016**, *302*, 33–41. [[CrossRef](#)]
29. Lü, Q.; Dong, X.; Zhu, Z.; Dong, Y. Environment-oriented low-cost porous mullite ceramic membrane supports fabricated from coal gangue and bauxite. *J. Hazard. Mater.* **2014**, *273*, 136–145. [[CrossRef](#)]
30. Yun, Y.; Gao, R.; Yue, H.; Liu, X.; Li, G.; Sang, N. Polycyclic aromatic hydrocarbon (PAH)-containing soils from coal gangue stacking areas contribute to epithelial to mesenchymal transition (EMT) modulation on cancer cell metastasis. *Sci. Total Environ.* **2017**, *580*, 632–640. [[CrossRef](#)]
31. Li, J.; Wang, J. Comprehensive utilization and environmental risks of coal gangue: A review. *J. Clean. Prod.* **2019**, *239*, 117946. [[CrossRef](#)]
32. Qiu, G.; Luo, Z.; Shi, Z.; Ni, M. Utilization of coal gangue and copper tailings as clay for cement clinker calcinations. *J. Wuhan Univ. Technol. Mater. Sci. Ed.* **2011**, *26*, 1205–1210. [[CrossRef](#)]
33. Jiang, X.; Lu, W.X.; Zhao, H.Q.; Yang, Q.C.; Yang, Z.P. Potential ecological risk assessment and prediction of soil heavy-metal pollution around coal gangue dump. *Nat. Hazards Earth Syst. Sci.* **2014**, *14*, 1599–1610. [[CrossRef](#)]
34. Marchon, D.; Kawashima, S.; Bessaies-Bey, H.; Mantellato, S.; Ng, S. Hydration and rheology control of concrete for digital fabrication: Potential admixtures and cement chemistry. *Cem. Concr. Res.* **2018**, *112*, 96–110. [[CrossRef](#)]
35. Zhou, W.; Du, H.; Kang, L.; Du, X.; Shi, Y.; Qiang, X.; Li, H.; Zhao, J. Microstructure evolution and improved permeability of ceramic waste-based bricks. *Materials* **2022**, *15*, 1130. [[CrossRef](#)]
36. Valencia, L.; Rosas, W.; Aguilar-Sanchez, A.; Mathew, A.P.; Palmqvist, A.E. Bio-based micro-/meso-/macroporous hybrid foams with ultrahigh zeolite loadings for selective capture of carbon dioxide. *ACS Appl. Mater. Interfaces* **2019**, *11*, 40424–40431. [[CrossRef](#)] [[PubMed](#)]
37. Jiang, N.; Shen, Y.; Liu, B.; Zhang, D.; Tang, Z.; Li, G.; Fu, B. CO₂ capture from dry flue gas by means of VPSA, TSA and TVSA. *J. CO₂ Util.* **2020**, *35*, 153–168. [[CrossRef](#)]
38. Zhou, C.; Alshameri, A.; Yan, C.; Qiu, X.; Wang, H.; Ma, Y. Characteristics and evaluation of synthetic 13X zeolite from Yunnan's natural halloysite. *J. Porous Mater.* **2013**, *20*, 587. [[CrossRef](#)]
39. Hedin, N.; Chen, L.J.; Laaksonen, A. Sorbents for CO₂ capture from flue gas—Aspects from materials and theoretical chemistry. *Nanoscale* **2010**, *2*, 1819–1841. [[CrossRef](#)]
40. Wilke, A.; Weber, J. Hierarchical nanoporous melamine resin sponges with tunable porosity—Porosity analysis and CO₂ sorption properties. *J. Mater. Chem.* **2011**, *21*, 5226–5229. [[CrossRef](#)]
41. Han, Y.; Hwang, G.; Kim, H.; Haznedaroglu, B.Z.; Lee, B. Amine-impregnated millimeter-sized spherical silica foams with hierarchical mesoporous–macroporous structure for CO₂ capture. *Chem. Eng. J.* **2015**, *259*, 653–662. [[CrossRef](#)]

42. Chen, H.; Zhang, Y.J.; He, P.Y.; Li, C.J. Synthesis, characterization and modification of monolithic ZSM-5 from geopolymer for CO₂ capture: Experiments and DFT calculations. *Energy* **2019**, *179*, 422–430. [[CrossRef](#)]
43. Liu, Q.; He, P.; Qian, X.; Fei, Z.; Zhang, Z.; Chen, X.; Tang, J.; Cui, M.; Qiao, X.; Shi, Y. Enhanced CO₂ adsorption performance on hierarchical porous ZSM-5 zeolite. *Energy Fuels* **2017**, *31*, 13933–13941. [[CrossRef](#)]

Disclaimer/Publisher's Note: The statements, opinions and data contained in all publications are solely those of the individual author(s) and contributor(s) and not of MDPI and/or the editor(s). MDPI and/or the editor(s) disclaim responsibility for any injury to people or property resulting from any ideas, methods, instructions or products referred to in the content.